# Quantifying the width and angle of inclined cracks using laser-spot lock-in thermography

**J. Rodríguez-Aseguinolaza[1], M. Colom[1], J. González[1,2],**

**A. Mendioroz[1] and A. Salazar[1]\***

[1]Departamento de Física Aplicada I, Escuela de Ingeniería de Bilbao, Universidad del País Vasco UPV/EHU, Plaza Ingeniero Torres Quevedo 1, 48013 Bilbao, Spain.

[2]Department of Applied Physics, CINVESTAV Unidad Mérida, carretera Antigua a Progreso km 6, A.P. 73 Cordemex, Mérida Yucatán 97310, Mexico.

\*Corresponding author, E-mail address: agustin.salazar@ehu.es

**ABSTRACT**

In this work we introduce a method to determine the width and the orientation of tilted cracks. This method combines laser-spot lock-in thermography and calculations of the sample temperature by means of finite elements modelling. The fitting of the surface temperature, calculated from the numerical model, to experimental lock-in thermography data obtained by focusing the laser spot close to an artificial calibrated inclined crack delivers its width and angle. The agreement between nominal and retrieved values proves the ability of the method to size inclined cracks, even those of micrometric width.

**Keywords:** lock-in infrared thermography, nondestructive evaluation, cracks detection.

# 1. INTRODUCTION

Infrared (IR) thermography is a valuable tool to detect subsurface flaws in a non-contact manner [1]. In optically excited IR thermography, a light source delivers some energy to the inspected specimen producing a surface temperature rise. The temperature gradient produced by the absorbed energy induces heat diffusion in the material. Abnormal temperature regions in the thermogram witness the presence of inner defects. Halogen or flash lamps, illuminating the whole sample surface uniformly, produce an in-depth heat flux, which is well adapted to image defects parallel to the surface, such as corrosion or delaminations. On the other hand, if a laser beam is focused at the sample surface (laser-spot), in addition to the in-depth propagation, the excitation induces a lateral heat flux, which is disturbed by the presence of a surface breaking crack. As a result, an abrupt temperature discontinuity appears in the thermogram along the length of the fissure. Scanning the laser-spot along the sample surface at constant velocity while recording the temperature by an IR camera (the so-called flying spot thermography) is a fast way to image the length of surface breaking cracks [2-16].

Once detected, the width and depth of a vertical crack can be sized accurately by bringing the laser spot close to the crack, and fitting the theoretical expression of the surface temperature to the experimental data. The best signal to noise ratio is obtained with lock-in thermography, where the laser beam is harmonically modulated at a given frequency and the amplitude of the temperature oscillation is recorded by the IR camera. This lock-in procedure can reduce the noise level far below the thermal sensitivity of any state of the art infrared camera (20 mK) [17].

In the case of infinite vertical cracks, an analytical expression of the surface temperature can be obtained, which has been used to size the width of artificial calibrated fissures [18]. For vertical cracks of finite depth, instead, the surface temperature must be obtained numerically. Several research groups have used finite elements modelling (FEM) to solve the heat diffusion equation to simulate the surface temperature of a sample containing a finite vertical crack and to size its depth [19-29].

However, in many cases the crack does not lie perpendicular to the surface, but inclined with an angle. This is the case of defects in rolling or forging laps [30-33]. Rolling contact fatigue cracks develop from the surface and usually propagate at their early stage making a small angle with the surface [34,35]. With the aim of covering all possible crack orientations and generalize the characterization of fatigue cracks beyond vertical fissures, in this work we address the challenge of sizing the width and angle of inclined infinite cracks using laser-spot lock-in thermography. First, using FEM, we develop a code to simulate the temperature of a sample containing a tilted planar infinite fissure making an arbitrary angle with the surface when a modulated laser beam hits the sample surface close to the crack. Then, we use this code to perform a sensitivity analysis to verify whether both quantities, width and angle, are uncorrelated in the surface temperature and hence they can be obtained simultaneously from the same amplitude thermogram. Finally, we verify the validity of the method by performing laser-spot lock-in thermography experiments on samples containing artificial calibrated inclined infinite cracks.

# 2. THEORY

In this section, we explain the method to calculate the temperature of a sample containing an infinite in depth inclined crack, which is illuminated by a harmonically modulated laser spot. Figure 1a shows the configuration, where $l$ is the distance between the center of the laser spot and the crack, $w$ is the width of the crack and $\theta$ is the angle of the crack with respect to the surface. We assume that the laser beam has a Gaussian profile, it is focused to a radius $a$

(at $1/e^2$ of the maximum intensity) and its center is located on the $y$-axis $(0,l,0)$. The laser power is $P_o$ and its amplitude is modulated at a frequency $f$ ($\omega = 2\pi f$): $P_o = P_o[1+\cos(\omega t)]$. The resulting sample temperature is the superposition of the ambient temperature, a stationary temperature rise and a temperature oscillation at the same frequency $f$ as the illumination. In lock-in thermography we are interested only in the temperature oscillation, $T$, which satisfies the heat diffusion equation together with heat flux continuity at the sample surface and at the crack surface, and temperature discontinuity at the crack position

$$\nabla^2 T(\vec{r},t) - \frac{1}{D}\frac{\partial T(\vec{r},t)}{\partial t} = 0, \tag{1}$$

$$-K\frac{\partial T(\vec{r},t)}{\partial z}\bigg|_{z=0} = \frac{\eta P_o}{\pi a^2}e^{-\frac{2r^2}{a^2}}\cos(\omega t), \tag{2}$$

$$[\![K\nabla T(\vec{r},t)]\!]\big|_{crack} = 0, \tag{3}$$

$$\Delta T(\vec{r},t)\big|_{Crack} = R_{th}K\nabla T(r,t)\big|_{Crack}. \tag{4}$$

Here $\eta$ is the power fraction absorbed by the sample, and $K$ and $D$ are thermal conductivity and diffusivity, respectively. The [[ ]] operator stands for the change on the flux over the crack. In Eq. (2) we have neglected heat losses by convection and radiation. This assumption is valid provided the amplitude of the temperature oscillation of the sample is small. In this way, adiabatic boundary conditions are taken for the remaining sample surfaces. Note that in Eq. (4) the crack is modeled as a surface with a thermal contact resistance, $R_{th}$, which is related to the crack width through the following expression [36]

$$R_{th} = \frac{w}{K_{air}}. \tag{5}$$
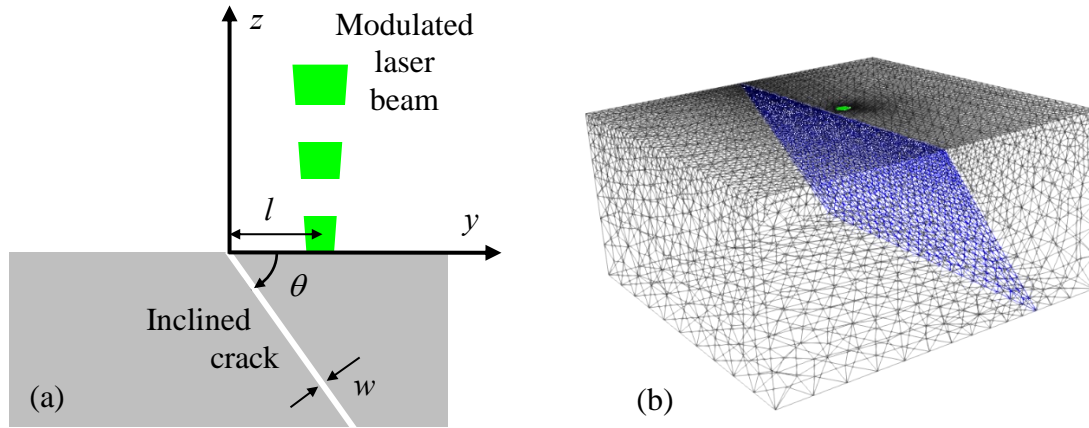


**Figure 1.** (a) Cross section of the sample containing an infinite inclined crack. (b) Triangulation of the sample domain. The crack is depicted in blue as a 2-D interface, whereas the laser heat supply is depicted as a green circle. For the sake of clarity, only the surface mesh is represented.

Eqs. (1) to (4) have analytical solutions only for an infinite vertical ($\theta = 90°$) crack [18]. In the case of an inclined crack, we have to proceed numerically, using FEM. As it is well known, FEM provide a solution to the model equations over a spatial triangulation of the studied domain. This one is usually modeled as a transmission problem in a material consisting of two domains, the bulk and the air filling the crack. This modeling strategy requires the meshing of the full domain, including the crack, which implies very fine spatial discretization inside the

crack volume. Therefore, for very thin cracks this model requires excessively fine meshes, dramatically increasing memory resources and computing time. To overcome this problem, we modeled the crack as a temperature jump over the grid nodes of the crack (see Fig. 1b). As can be seen, the centered and densely discretized area corresponds to the iluminated zone around the center of the laser spot, where the boundary condition (Eq. 2) is applied in a circle of a radius $2a$ in the numerical discretization. This election guarantees that outside this circle the intensity of the gaussian excitation is negligible. We have developed a code to simulate the temperature oscillation of a sample containing a inclined crack.

This temperature depends on the thermal properties of the sample ($D$ and $K$), on the laser characteristics ($\eta$, $P_o$, $a$ and $f$) and on the crack parameters ($l$, $\theta$ and $R_{th}$). Anyway, according to Eq. (2), $T$ depends on the ratio $\eta P_o/K$, indicating that for a given laser power the amplitude of the temperature oscillation is high for poor thermal conductors. On the other hand, according to Eq. (3) the temperature discontinuity at the crack depends on the product $KR_{th} = Kw/K_{air}$ (see Eq. (4)), indicating that for a given crack width the temperature jump at the crack is large for good thermal conductors or equivalently, it is much easier to detect narrow cracks in good thermal conductors than in insulators.

## 3. SIMULATIONS AND SENSITIVITY ANALYSIS

The solution of Eqs. (1) to (4) gives the temperature oscillation, which is harmonically time-dependent. In order to obtain the amplitude of this oscillation, |$T$|, which is the quantity recorded in experiments from a lock-in analysis, a complete thermal cycle needs to be simulated. In Fig. 2a we show the simulations of the amplitude of the temperature profile along the $y$-axis (perpendicular to the crack, through the center of the laser spot) for a sample made of stainless steel AISI-304 ($D = 4$ mm$^2$/s, $K = 15$ Wm$^{-1}$K$^{-1}$), which is illuminated by a Gaussian laser beam of radius $a = 0.2$ mm, whose center is located at a distance $l = 0.4$ mm from the crack. The laser power is $P_o = 0.1$ W ($\eta = 1$) and the modulation frequency is $f = 0.8$ Hz. The crack width is the same in all cases, $w = 5$ μm, and seven crack angles are analyzed. We plot the natural logarithm of the amplitude rather than the amplitude itself to better resolve the curves far away from the excitation, where the temperature features low values, as those produced at the non-illuminated side of the crack. As can be observed, varying the crack angle produces a small change on the temperature profile. In particular, for $\theta < 90°$ the effect is concentrated at the illuminated side of the sample ($y > 0$), while the non-illuminated branch of the profile ($y < 0$) remains insensitive. On the contrary, for $\theta > 90°$ the effect is more pronounced at the non-illuminated side of the sample ($y < 0$), while the illuminated branch of the profile ($y > 0$) remains unchanged. In Fig. 2b we show the effect of varying the crack width while the angle is kept fixed ($\theta = 45°$). Simulations have been performed using the same thermal and geometrical parameters as in Fig. 2a. As can be observed, changing the crack width drastically affects the temperature discontinuity at the crack position. Figs. 2a and 2b indicate that ln|$T$| is more sensitive to $w$ than to $\theta$. Therefore, it is expected that using a laser-spot lock-in thermography setup $w$ will be obtained with a higher precision than $\theta$.

Nevertheless, as we are interested in measuring both parameters, $w$ and $\theta$, accurately, we have to verify that they are not correlated, i.e. only a single ($w$, $\theta$) couple can reproduce a given temperature profile, and therefore, that $w$ and $\theta$ can be determined univocally from the same amplitude thermogram. In order to settle this issue, we have calculated the sensitivity of ln|$T$| to $w$ and $\theta$ according to the following definition

$$S_j = j\frac{\partial\left[\ln|T|\right]}{\partial j}, \qquad j = w, \theta. \tag{6}$$

4

In Fig. 3 we plot the simulation of the sensitivity of $\ln|T|$ along the $y$-profile to both parameters in the case of a typical crack: $w = 5$ µm and $\theta = 45°$. The sensitivity to the width ($S_w$) is shown in black and the sensitivity to the depth ($S_\theta$) in red. Simulations have been performed for AISI-304 with the same experimental parameters as in Fig. 2: $\eta = 1$, $P_o = 0.1$ W, $f = 0.8$ Hz, $a = 0.2$ mm and $l = 0.4$ mm. As can be observed, both quantities are not correlated since their sensitivities are not proportional and therefore they can be obtained univocally from one temperature profile. Note that the sensitivity to the width is concentrated at the non-illuminated side of the crack, whereas the sensitivity to the angle appears at the illuminated side. Anyway, it is confirmed that, as it was already suggested by Fig. 2, $S_\theta < S_w$.
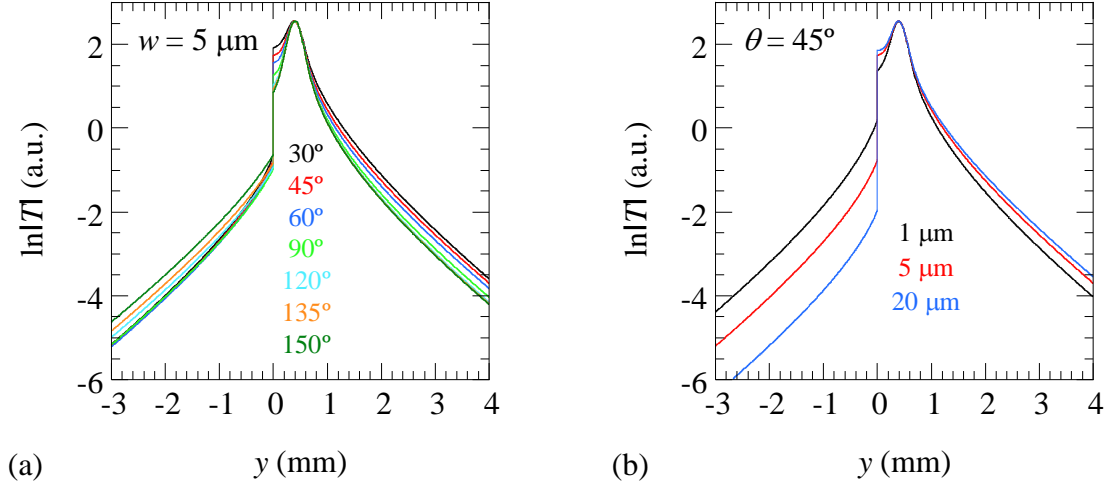


**Figure 2.** Simulation of $\ln|T|$ as a function of the transverse distance to a crack, located at $y = 0$. (a) Same crack width, $w = 5$ µm, and different inclinations. (b) Same angle with the surface, $\theta = 45°$, and three different widths. Simulations have been performed for AISI-304 with the following experimental parameters: $\eta = 1$, $P_o = 0.1$ W, $f = 0.8$ Hz, $a = 0.2$ mm and $l = 0.4$ mm.
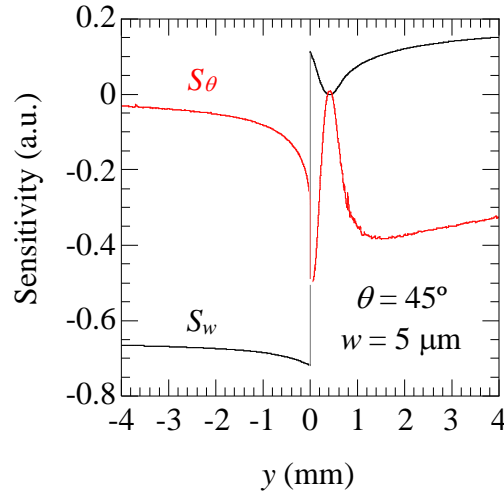


**Figure 3.** Simulation of the sensitivity of $\ln(|T|)$ to the width, $S_w$, and to the angle, $S_\theta$, for a 5 µm wide crack making an angle $\theta = 45°$ with the surface. Simulations have been performed for an AISI-304 sample with the same experimental parameters as in Fig. 2.

## 4. EXPERIMENTS AND DISCUSSION

In Fig. 4a we show a scheme of the laser-spot lock-in thermography setup. A CW laser (532 nm, up to 6 W) of Gaussian profile is modulated by a mechanical chopper and focused onto the sample surface down to a radius of about 200 μm by means of a spherical lens of 10 cm focal length. A Ge window, which is opaque to visible light, reflects the laser beam and allows directing it perpendicularly to the specimen. At the same time, this Ge window is transparent to the IR radiation allowing the thermal energy emitted by the sample to reach the IR video camera. The camera (3-5 μm, 256×320 px, 30 μm pitch, up to 380 images/s at full frame, NETD 20 mK), synchronized with the chopper, records the surface temperature oscillations for several seconds. A lock-in module analyses the recorded film at the modulation frequency and delivers a temperature amplitude thermogram. Typically, we analyze 10,000 images in the lock-in process, which reduces the noise level in amplitude down to 1 mK. A macro lens produces a magnification ratio 1:1, i.e. each pixel of the detector senses the average temperature over a 30 μm square of the sample. The sample is mounted on a micro-positioning system to control the distance between the laser spot and the fissure.

To test the validity of laser-spot lock-in thermography to measure the width and angle of tilted cracks we have manufactured inclined cracks with calibrated width and angle by sandwiching two metallic tapes of the same thickness (5, 10 and 20 μm) between two stainless steel AISI-304 ($D = 4$ mm$^2$/s, $K = 15$ Wm$^{-1}$K$^{-1}$), wedged blocks (see Fig. 4b). Three block couples have been prepared with three wedge angles: 30°, 45° and 60°. All surfaces in contact were polished to guarantee a good thermal coupling in the absence of tapes. Some pressure was applied to the blocks in contact to assure that the tapes thickness is close to the fissure width. A very thin graphite layer was deposited at the front surface of the coupled blocks to reduce the laser reflectivity and to enhance the infrared emissivity. Moreover, this graphite layer reduces surface heterogeneities, which disturb the temperature profiles.
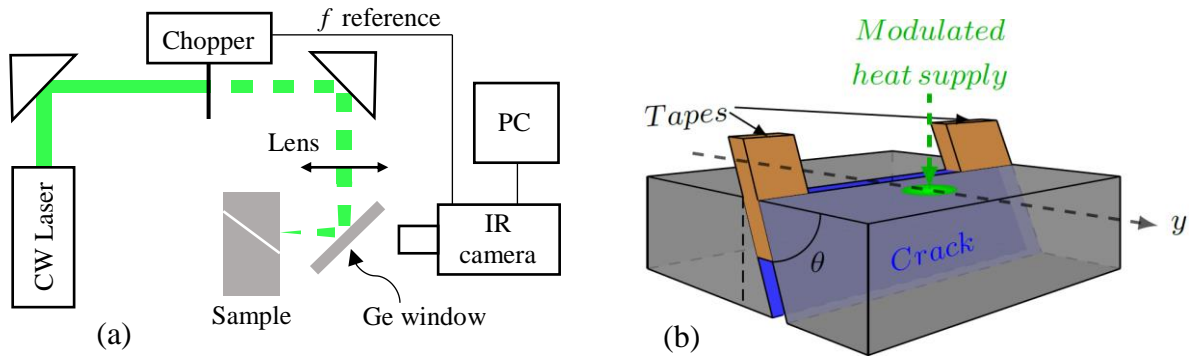


**Figure 4.** (a) Scheme of the laser-spot lock-in thermography setup. (b) Diagram of the inclined crack simulated for the experiment: two thin metallic tapes of thickness *w* are sandwiched between two wedge blocks of AISI-304 stainless steel.

In order to obtain the width and angle of the crack, we fit the numerical model to the experimental temperature profiles along the *y*-axis, i.e. the straight-line perpendicular to crack and crossing the center of the laser spot. As explained in the previous section, this temperature profile depends on the following seven parameters: $D$, $\eta P_o/K$, $KR_{th}$, $a$, $f$, $l$ and $\theta$. The thermal properties of the sample are known. The modulation frequency is selected by the researcher. The laser radius and the distance between laser and crack are measured optically. All experimental temperature profiles are normalized to the value at the center of the laser spot:

$T_n(y)= T(y)/T(l)$, leading to $\eta P_o/K$ independent results. Accordingly, the remaining two free parameters for the fitting procedure are: $R_{th}$ and $\theta$. Moreover, according to Eq. (5), $R_{th}$ can be replaced by $w$, whose value is easier to grasp than that of the thermal resistence.

In Fig. 5 we represent the normalized experimental temperature profiles for the three angles (30º, 45º and 60º) and their supplementary (150º, 135º and 120º). For each angle four nominal crack widths (0, 5, 10 and 20 µm) have been studied. 0 µm means that we put the two blocks directly in contact. Experiments have been performed at $f = 0.8$ Hz. For the sake of clarity, the normalized temperature profiles have been shifted vertically. Dots are the experimental results and the continuous lines the fittings to the model. Note the low noise of the experimental data and the good quality of the fittings.

The retrieved values of $w$ and $\theta$ are summarized in Table 1. As can be observed, for all angles, even though the two blocks are in direct contact (i.e. nominal width $w = 0$ µm) there is a clear jump in temperature indicating that the thermal contact is not perfect. The retrieved widths are in the range 1.5-3 µm. These values are higher than those obtained for vertical cracks ($\theta = 90º$), which are typically below 1 µm [18]. This is because in the manufacturing process it is more difficult to keep the parallelism in wedge blocks than in orthogonal ones. This offset is kept for wider cracks: e.g. for nominal $w = 5$ and 10 µm, the obtained values are in the range 7-10 µm and 13-16 µm, respectively. Notice that the uncertainty in $w$ is about 5% for angles smaller than 90º, what is remarkably low for this quantity. However, for $\theta > 90º$ the uncertainty in $w$ grows as we move from 120º to 150º.

Regarding the angle, as can be observed in Table 1, all retrieved angles suffer from a deviation from the nominal value. For $\theta < 90º$ there is a slight systematic overestimation, whereas for $\theta > 90º$ the angle is underestimated. This deviation must be ascribed to the measurement procedure itself since, unlike the case of the width, the angle of the wedge is manufactured with a precision better than 0.1º. On the other hand, the uncertainty in $\theta$ is higher than the uncertainty in $w$, as it was predicted by the sensitivity analysis performed in section 2.

In order to visualize the origin of the higher uncertainty of the obtained values of $w$ and $\theta$ for $\theta > 90º$ we have plotted in Fig. 6 the root-mean-square error (RMSE) corresponding to the fittings in Fig. 5 for $w = 10$ µm and two supplementary angles: 45º and 135º. In the case of $\theta = 45º$ we have plotted the RMSE values obtained by fixing the value of the angle (starting at 35º and growing by 1º up to 65º), and fitting the crack width. Similarly, for $\theta = 135º$ we have plotted the RMSE values obtained for fixed angles (starting at 100º and growing by 2º up to 150º) and fitting the width as the only fitting parameter. As can be observed, for both angles there is a minimum corresponding to the couple $(w,\theta)$ producing the best fitting of the experimental data. However, for $\theta = 45º$ the minimum is sharp and well-defined indicating a low uncertainty in the retrieved values of $w$ and $\theta$. On the contrary, for $\theta = 135º$ the minimum is flat leading to a higher uncertainty in $w$ and $\theta$.

These evidences bring us to conclude that the optimum configuration to determine the crack inclination and width consists in exciting the side that is above the tilted crack. In these conditions, reliable and precise values of both the width and angle with the surface are retrieved, although the latter is slightly overestimated.
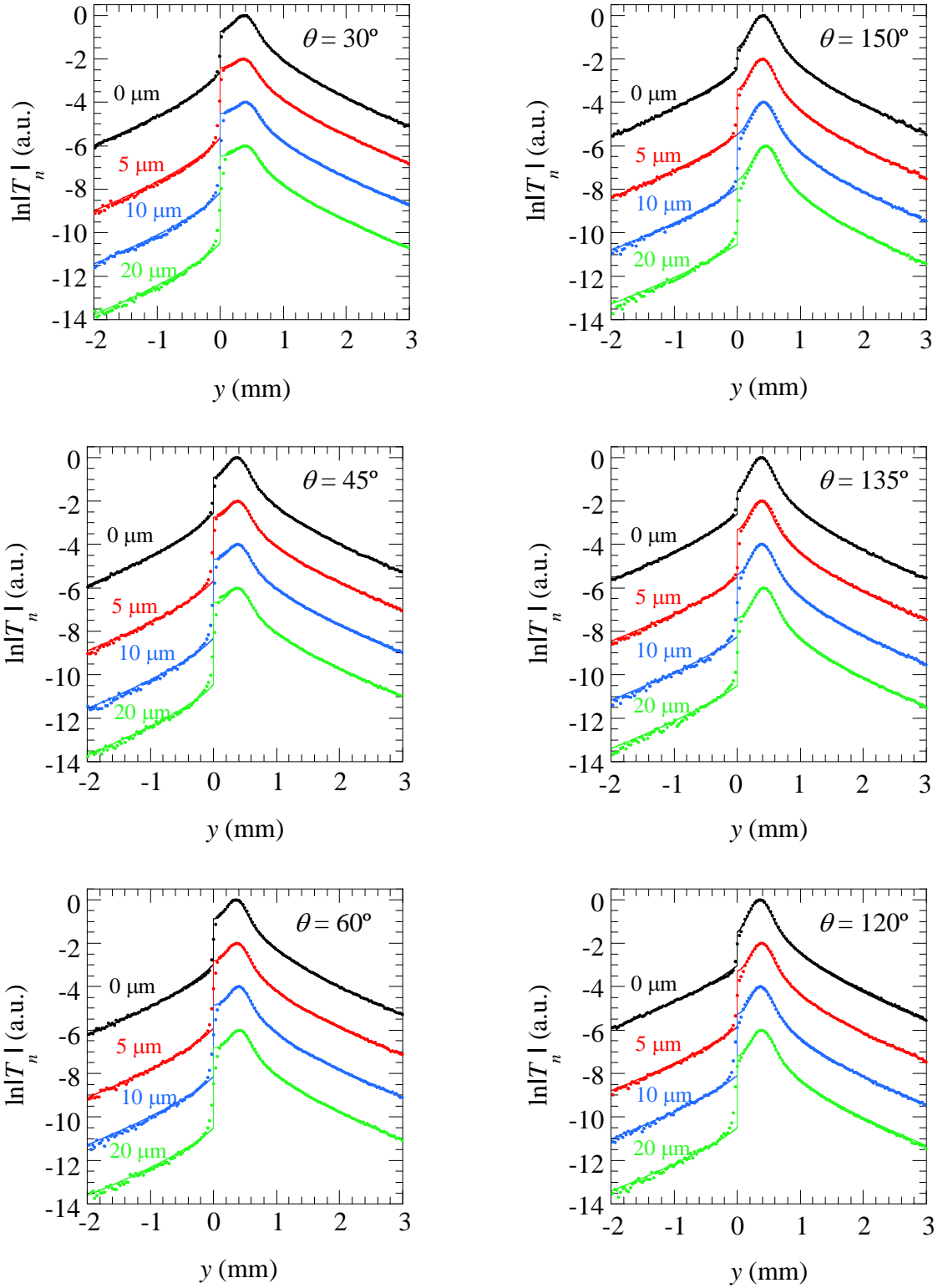
**Figure 5.** Normalized experimental $\ln|T_n|$ profiles at $f = 0.8$ Hz. Dots are the experimental results and the continuous line is the fitting to the model. For the sake of clarity, the profiles for different widths have been shifted. The values of the width and angle are the nominal ones.
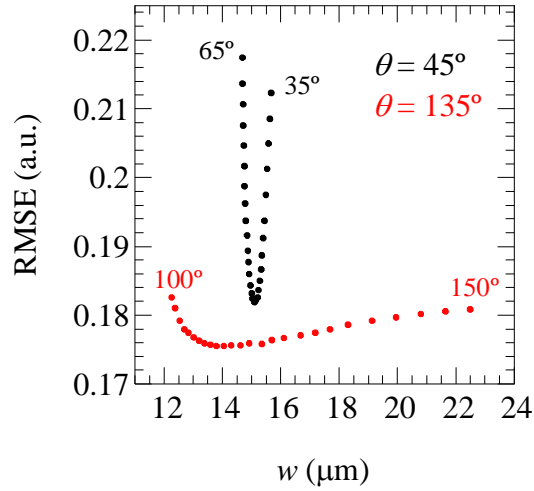
**Figure 6.** RMSE values corresponding to the fittings in Fig. 5 for $w = 10$ μm and two complementary angles: 45º and 135º.

In this work we have used lock-in thermography because this technique provides a high signal to noise ratio leading to very clean temperature profiles, even if the temperature is plotted in a logarithmic scale, which allows detecting low temperature differences. However, it is worth noting that pulse thermography, which makes use of a brief laser pulse to excite the sample and the infrared camera records the temperature evolution of the sample surface, could be used as an alternative to lock-in thermography. Actually, pulse thermography has already been used to size the width of vertical cracks by fitting the theoretical model to the experimental temperature profiles [37]. Although pulse thermography gives a lower signal to noise ratio, the signal processing is easier and might be better suited to the industrial environment.

**Table 1.** Summary of the obtained values of width and angle ($w, \theta$) of the artificial inclined cracks dealt with in this work.

| Nominal $\theta$ / Nominal $w$ | 30° | 45° | 60° | 120° | 135° | 150° |
|---|---|---|---|---|---|---|
| 0 μm | $w = 2.2\pm0.2$ μm $\theta = 35\pm5°$ | $w = 1.7\pm0.2$ μm $\theta = 50\pm3°$ | $w = 3.1\pm0.2$ μm $\theta = 66\pm5°$ | $w = 3.2\pm0.4$ μm $\theta = 150\pm6°$ | $w = 2.3\pm0.5$ μm $\theta = 150\pm10°$ | $w = 1.2\pm0.5$ μm $\theta = 130\pm10°$ |
| 5 μm | $w = 9.2\pm0.4$ μm $\theta = 30\pm3°$ | $w = 7.7\pm0.3$ μm $\theta = 49\pm5°$ | $w = 9.5\pm0.4$ μm $\theta = 62\pm3°$ | $w = 8.7\pm0.4$ μm $\theta = 110\pm7°$ | $w = 6.3\pm0.7$ μm $\theta = 120\pm10°$ | $w = 7\pm4$ μm $\theta = 130\pm20°$ |
| 10 μm | $w = 15.2\pm0.6$ μm $\theta = 35\pm5°$ | $w = 15.1\pm0.4$ μm $\theta = 48\pm5°$ | $w = 12.2\pm0.6$ μm $\theta = 60\pm3°$ | $w = 11.7\pm0.5$ μm $\theta = 110\pm7°$ | $w = 13.9\pm1.3$ μm $\theta = 120\pm10°$ | $w = 12\pm8$ μm $\theta = 135\pm15°$ |
| 20 μm | $w = 22.0\pm0.8$ μm $\theta = 35\pm5°$ | $w = 18.5\pm0.8$ μm $\theta = 51\pm5°$ | $w = 18.6\pm0.8$ μm $\theta = 62\pm3°$ | $w = 18.0\pm1.0$ μm $\theta = 100\pm10°$ | $w = 16\pm3$ μm $\theta = 110\pm15°$ | $w = 20\pm11$ μm $\theta = 135\pm20°$ |

## 5. CONCLUSIONS

Lock-in infrared thermography has been proven as an efficient contactless and quantitative tool to determine the inclination and width of infinite surface breaking cracks. The methodology involves the fitting of the amplitude of the surface temperature oscillation obtained using FEM to experimental laser-spot lock-in thermography data.

The sensitivity analysis based on FEM confirms that the inclination and the width of the crack are not correlated in the amplitude profile perpendicular to the crack through the center of the laser spot, and thus that both crack characteristics (width and inclination) can be obtained univocally from a single amplitude thermogram. The analysis also reveals a higher sensitivity to the width than to the inclination. The method has been tested by taking laser-spot lock-in thermography data on samples containing artificial and calibrated tilted cracks, making different angles with the surface that range between 30º and 150º. The results indicate that the crack width is retrieved with high accuracy and, as predicted by the sensitivity analysis, the uncertainty in the retrieved width is smaller than in the angle. Moreover, although for angles above 135º the uncertainty in the width increases, it stays rather robust (less than 5%) for angles smaller than 135º. On the contrary, the uncertainty of the retrieved angle is more affected by the value of the angle: the uncertainty is of about 5º for angles smaller than 90º (excitation above the crack) and it increases monotonically for increasing angles above 90º. Furthermore, the value of the angle is retrieved accurately if the inclination with the surface is less than 90º, but it is underestimated if the crack is tilted towards the non-illuminated side.

These results point out that, in order to determine the width and orientation of the crack accurately, it is advisable to excite the side of the fissure that is above the crack (angle with the surface smaller than 90º). As the overall orientation of the crack might be unknown beforehand, the proposed rule of thumb is: excite one side of the crack and, if the retrieved angle is higher than 90º, repeat the procedure exciting the other side of the crack. By proceeding this way, accurate and precise values of the crack width and inclination can be obtained.

As a future trend, let us remark that the FEM code developed in this manuscript can be easily implemented to deal with more realistic situations including finite tilted cracks and/or dealing with heat losses by convection and radiation that might be significant when analyzing cracks in low conductivity materials.

## ACKNOWLEDGMENTS

# REFERENCES

[1] X.P.V. Maldague, Theory and practice of infrared technology for nondestructive testing, John Wiley & Sons, New York (2001).

[2] E.J. Kubiak, Infrared detection of fatigue cracks and other near-surface defects, Appl. Opt. **7**, 1743-1747 (1968).

[3] Y.Q. Wang, P.K. Kuo, L.D. Favro and R.L. Thomas, A novel "flying-spot" infrared camera for imaging very fast thermal-wave phenomena, In Photoacoustic and Photothermal Phenomena II Springer Series in Optical Sciences **62**, 24-26 (1990).

[4] H.E. Cline and T.R. Anthony, Heat treating and melting material with scanning laser or electron beam, J. Appl. Phys. **48**, 3895 (1977).

[5] C. Gruss and D. Balageas, Theoretical and experimental applications of the flying spot camera, QIRT Conference Paris 1992. Available from QIRT Open Archives: http://dx.doi.org/10.21611/qirt.1992.004.

[6] J.L. Bodnar, M. Egée, C. Menu, R. Besnard, A. Le Blanc, M. Pigeon and J.Y. Sellier, Cracks detection by a moving photothermal probe, J. de Physique IV, Colloque C7 **4**, C7-591-594 (1994).

[7] J.C. Krapez, Résolution spatiale de la camera thermique à source volante, Int. J. Therm. Sci. **38**, 769-779 (1999).

[8] P.Y. Joubert, S. Hermosilla-Lara, D. Placko, F. Lepoutre and M. Piriou, Enhancement of open-crack detection in flying-spot photothermal non-destructive testing using physical effect identification, QIRT J. **3**, 53 (2006).

[9] J. Schlichting, M. Ziegler, A. Dey, Ch. Maierhofer and M. Kreutzbruck, Efficient data evaluation for thermographic crack detection, QIRT J. **8**, 119-123 (2011).

[10] T. Li, D.P. Almond and D.A.S. Rees, Crack imaging by scanning pulsed laser spot thermography, NDT&E Int. **44**, 216-225 (2011).

[11] S.E. Burrows, S. Dixon, S.G. Pickering, T. Li and D.P. Almond, Thermographic detection of surface breaking defects using scanning laser source, NDT&E Int. **44**, 589-596 (2011).

[12] A. Thiam, J.C. Kneip, E. Cicala, Y. Caulier, J.M. Jouvard and S. Mattei, Modeling and optimization of open crack detection by flying spot thermography, NDT&E Int. **89**, 67-73 (2017).

[13] D. Jiao, W. Shi, Z. Liu and H. Xie, Laser multi-mode scanning thermography method for fast inspection of micro-cracks in TBCs surface, J. Nondestr. Eval. **37**, 30 (2018).

[14] N. Montinaro, D. Cerniglia and G. Pitarresi, Evaluation of vertical cracks by means of flying laser thermography, J. Nondestr. Eval. **38**, 48 (2019).

[15] J. González, A. Mendioroz, A. Sommier, J.C. Batsale, C. Pradere and A. Salazar, Fast sizing of the width of infinite vertical cracks using Flying Spot thermography, NDT&E Int. **103**, 166-172 (2019).

[16] N. Puthiyaveettil, K.R. Thomas, S. Unnikrishnakurup, P. Myrach, M. Ziegler and K. Balasubramaniam, Laser line scanning thermography for surface breaking crack detection: modeling and experimental study. Infrared Phys. Technol. **104**, 103141 (2020).

[17] O. Breitenstein and M. Langenkamp, *Lock-in Thermography* (Springer, Berlin, 2003) p. 32.

[18] N.W. Pech-May, A. Oleaga, A. Mendioroz, A.J. Omella, R. Celorrio and A. Salazar, Vertical cracks characterization using lock-in thermography: I. Infinite cracks, Meas. Sci. Technol., **25**, 115601 (2014).

[19] J. Schlichting, Ch. Maierhofer and M. Kreutzbruck, Defect sizing by local excitation thermography, QIRT J. **8**, 51-63 (2011).

[20] J. Schlichting, Ch. Maierhofer and M. Kreutzbruck, Crack sizing by laser excited thermography, NDT&E Int. **45**, 133-140 (2012).

[21] M. Streza, Y. Fedala, J.P. Roger, G. Tessier and C. Boue, Heat transfer modelling for surface crack depth evaluation, Meas. Sci. Technol. **24**, 045602 (2013).

[22] Y. Fedala, M. Streza, J.P. Roger, G. Tessier and C. Boue, Open crack depth sizing by laser stimulated infrared lock-in thermography, J. Phys. D: Appl. Phys. **47**, 465501 (2014).

[23] C. Bu, Q. Tang, Y. Liu, X. Jin, Z. Sun and Z. Yan, A theoretical study on vertical finite cracks detection using pulsed laser spot thermography (PLST), Infrared Phys. Technol. **71**, 475-480 (2015).

[24] J. Qiu, C. Pei, H. Liu and Z. Chen, Quantitative evaluation of surface crack depth with laser spot thermography, Int. J. Fatigue **101**, 80-85 (2017).

[25] C. Boué and S. Holé, Open crack depth sizing by multi-speed continuous laser stimulated lock-in thermography, Meas. Sci. Technol. **28**, 065901 (2017).

[26] A. Scalbi, R. Olmi and G. Inglese, Evaluation of fractures in a concrete slab by means of laser-spot thermography, Int. J. Heat Mass Transf. **141**, 282-293 (2019).

[27] C. Boué and S. Holé, Comparison between multi-frequency and multi-speed laser lock-in thermography methods for the evaluation of crack depth in metal, QIRT J. **17**, 223-234 (2020).

[28] T. Ishizaki, T. Igami and H. Nagano, Measurement of local thermal contact resistance with a periodic heating method using microscale lock-in thermography, Rev. Sci. Instrum. **91**, 064901 (2020).

[29] M. Colom, J. Rodríguez-Aseguinolaza, A. Salazar and A. Mendioroz, Sizing the depth and width of narrow cracks in real parts by laser spot lock-in thermography, submitted for publication, 2020.

[30] Y. Kadin, A.V. Rychahivskyy, Modeling of surface cracks in rolling contact, Mater. Sci. Eng. A **541**, 143-151 (2012).

[31] U. Netzelmann, G. Walle, A. Ehlen, S. Lugin, M. Finckbohner and S. Bessert, NDT of Railway Components Using Induction Thermography, AIP Conf. Proc. **1706**, 150001 (2016).

[32] B. Oswald-Tranta, Induction thermography for surface crack detection and depth determination, Appl. Sci. **8**, 257 (2018).

[33] J. Peng, J. Bai, L. Feng and Z. He, The eddy current pulsed thermography detection of fatigue crack closure, AIP Conf. Proc. **2102**, 120002 (2018).

[34] Y. Fan, S. Dixon, R.S. Edwards and X. Jian, Ultrasonic wave propagation and interaction with surface defects on rail track crack, NDT&E Int. **40**, 471-477 (2007).

[35] I.Z. Abidin, G.Y. Tian, J. Wilson, S. Yang and D. Almond, Quantitative evaluation of angular defects by pulsed eddy current thermography, NDT&E Int. **43**, 537–546 (2010).

[36] H.S. Carslaw and J.C. Jaeger, *Conduction of Heat in Solids*, 2nd edition (Oxford University Press, 1959) p. 20.

[37] N.W. Pech-May, A. Oleaga, A. Mendioroz and A. Salazar, Fast Characterization of theWidth of Vertical Cracks Using Pulsed Laser Spot Infrared Thermography, J. Nondestruct. Eval. **35**, 22 (2016).